DoE Optimization Empowers the Automated Preparation of Enantiomerically Pure [^{18}F]Talazoparib and its *In Vivo* Evaluation as a PARP Radiotracer.

Gregory D. Bowden[†,#,‡], Sophie Stotz[†,#,‡], Johannes Kinzler[†], Christian Geibel[§], Michael Lämmerhofer[§], Bernd J. Pichler[†,#,^], and Andreas Maurer[†,#,*]

[†]Werner Siemens Imaging Center, Department of Preclinical Imaging and Radiopharmacy, Eberhard Karls University, Roentgenweg 15, 72076 Tuebingen, Germany

[#]Cluster of Excellence iFIT (EXC 2180) "Image-Guided and Functionally Instructed Tumor Therapies", Eberhard Karls University, Roentgenweg 13, 72076 Tuebingen, Germany

[§]Institute of Pharmaceutical Sciences, Department of Pharmaceutical (Bio-)Analysis, Eberhard Karls University, Auf der Morgenstelle 8, 72076 Tuebingen, Germany

^German Cancer Research Center, German Cancer Consortium DKTK, Partner Site Tuebingen, Roentgenweg 13, 72076 Tuebingen, Germany

KEYWORDS: Talazoparib, Radiolabeling, Radiotracer, Copper-mediated radiofluorination, Design of Experiments, Chiral separation, PET Imaging, Biodistribution

GRAPHICAL ABSTRACT

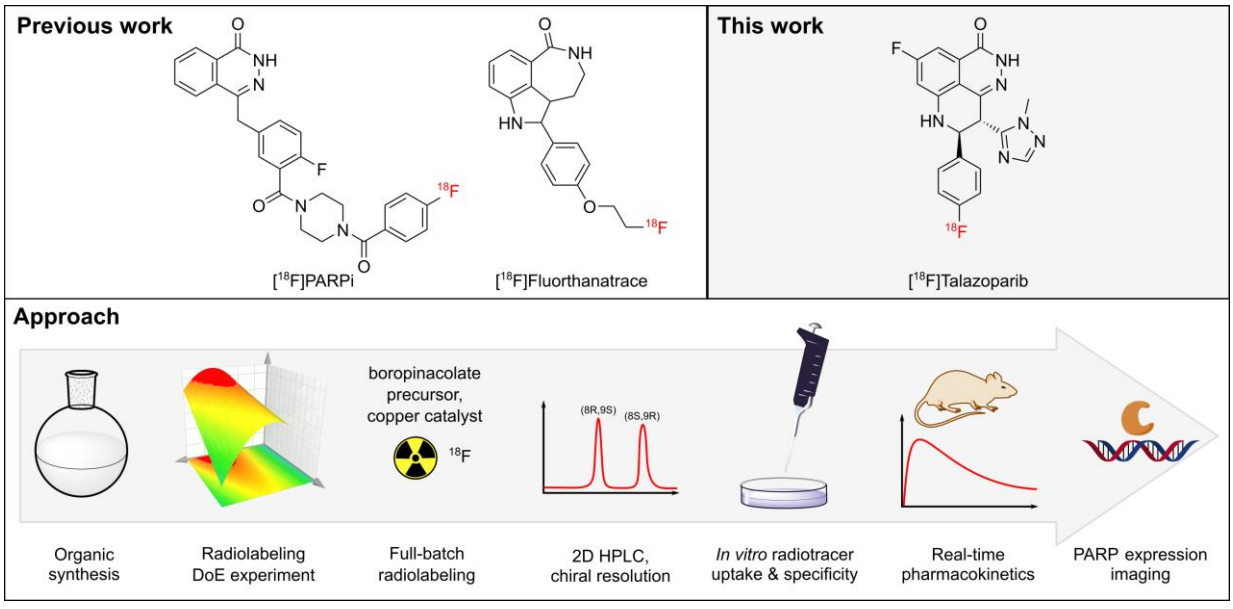

ABSTRACT: PARP inhibitors are proven chemotherapeutics and serve as lead structures for the development of PARP-targeted *in vivo* imaging probes. Given the clinical potential of PARP imaging for the detection and stratification of various cancers, the development of novel PARP imaging probes with improved pharmacological profiles over established PARP imaging agents is warranted. Here, we present a novel ^{18}F-labeled PARP radiotracer based on the clinically superior PARP inhibitor talazoparib. An automated radiosynthesis of [^{18}F]talazoparib (RCY: 13 ± 3.4 %; n = 4; molar radioactivity 52 – 176 GBq/µmol) was achieved using a "Design of Experiments" (DoE) optimized copper-mediated radiofluorination reaction. The chiral product was isolated from the reaction mixture using 2D reversed-phase/chiral radio-HPLC (>99% ee). (8S, 9R)-[^{18}F]Talazoparib demonstrated PARP binding in HCC1937 cells *in vitro* and showed an excellent tumor-to-blood ratio in xenograft-bearing mice (10.2 ± 1.5). Despite expected uptake into muscle, bone, and abdominal tissue, a favorable pharmacological profile in terms of excretion, blood half-life, and target engagement was observed in the pilot *in vivo* study. This synthesis of [^{18}F]talazoparib exemplifies how a DoE based tracer development pipeline can enable the radiosyntheses of clinically relevant but synthetically challenging radiolabeled compounds of high interest to the imaging community.

INTRODUCTION

Poly(ADP-ribose) polymerases (PARP) have become important targets for personalized cancer treatment, and this has spurred the development of several highly potent PARP inhibitors. PARP inhibitors induce synthetic lethality in malignant tumors that lack the homologous recombination (HR) DNA repair pathway.[1-2] PARP overexpression in several tumor entities has also made the enzyme a valuable biomarker for optical and nuclear imaging techniques to detect malignant lesions and aid surgical excision of difficult-to-detect cancers.[3] Non-invasive imaging techniques such as positron emission tomography (PET) are used to track the fate and quantify the uptake of a radioactively labeled molecule *in vivo;* thus, aiding diagnosis and therapy surveillance. PARP expression levels are thought to be predictive of tumor malignancy, as its overexpression is correlated with a poor clinical prognosis.[4-6]

The PARP enzyme family consists of 17 members, of which PARP1 is the most abundant and best-characterized. It senses DNA single-strand breaks (SSBs) with its zinc finger domains and initiates their repair upon auto poly(ADP-ribosyl)ation (PARylation), which recruits repair enzymes.[7-9] PARP1, PARP2, and PARP5a and b (tankyrase 1 and 2) are capable of PAR chain formation while the remaining PARP enzymes can perform mono(ADP-ribosyl)ation (MARylation) or are enzymatically inactive.[10,11]

The catalytic domains of PARP enzymes use nicotinamide adenine dinucleotide (NAD^+) as the substrate for PARylation.[12-13] PARP inhibitors structurally mimic NAD^+, thus blocking the catalytic domain and escalating the SSBs to double-strand breaks (DSBs) that can only be repaired by alternative DNA repair mechanisms like HR.[14] In addition to their catalytic inhibition, some PARP inhibitors are (to various extents) able to trap the PARP enzyme on the damaged DNA site, leading to replication fork collapse and ultimately cell death.[15]

Within the last decade, numerous PARP inhibitors with various levels of cytotoxic efficacy have been approved by the U.S. Food and Drug Administration (FDA): olaparib (2014), rucaparib (2016), niraparib (2017), and talazoparib (2018).[16-19] These inhibitors are mainly used in combination with DNA damaging agents like cisplatin in HR-deficient cancer entities or for maintenance therapy. Several ongoing studies are also exploring the potential of PARP inhibitors for monotherapy in HR-potent tumors.[20] It is commonly agreed that the substantial differences in the cytotoxic effica-

cies of the known PARP inhibitors are explained by the differences in their abilities to trap PARP1 on damaged DNA and not necessarily by their binding affinities alone.[21]

Talazoparib is considered the most potent of the known PARP1 inhibitors and the best PARP trapping agent.[21-23] The molecule possesses two distinct chiral centers. Of the four possible stereoisomers, the *trans* enantiomers are present as the two dominant diastereomers. The (8S, 9R)-diastereomer (talazoparib) is an excellent PARP inhibitor, while its enantiomer ((8R, 9S) LT-674) is less active by several orders of magnitude, along with the other diastereomers.[24] It has been proposed that the bulky structure and stereochemistry of talazoparib contribute to its high potency, although the exact nature of the molecular interaction remains elusive.[25]

PARP imaging has proven its exceptional clinical merit in several scenarios, specifically for the detection and delineation of oral, brain, pancreatic, and liver cancers, as well as target engagement imaging of different PARP inhibitors.[26-32] Several PARP1-targeted imaging probes have been developed, with the most prominent among these being PARPi-FL, a fluorescently labeled olaparib analog; [^{18}F]PARPi, PARPi-FL's radioactive sibling; [^{18}F]olaparib, isotopically radiolabeled olaparib; and [^{18}F]FTT, the first clinically applied PARP radiotracer based on rucaparib.[33] To fully exploit PARP as an imaging biomarker, the development of novel PARP imaging probes with further improved pharmacological profiles is warranted. To our knowledge, no radiotracer based on talazoparib has been published to date, despite its potential as a superior next-generation PARP imaging probe.

Given the short half-life of ^{18}F-fluorine (109.8 minutes), the synthesis of enantiomerically pure and isotopically radiolabeled [^{18}F]talazoparib represents a complex radiosynthetic challenge. An accessible radiosynthesis of [^{18}F]talazoparib has become possible because of the recent advances in radiochemical methodology such as copper-mediated radiofluorination chemistry (CMRF).[34-37] Our previous works have explored this methodology by using the "Design of Experiments" (DoE) approach to reaction optimization, and this has helped us lay the foundation of a DoE based radiotracer development pipeline using CMRF chemistry.[38-39] DoE aids in establishing reliable and robust radiosyntheses from the onset of the tracer development process and, in combination with the "de-risking" strategies described by Taylor *et al.*, this approach can be used to expedite the development of novel radiotracers.[40] In this work, we successfully applied a refined DoE based tracer development workflow to the challenging radiosynthetic problem of [^{18}F]talazoparib. Here we present an efficient automated radiosynthesis of enantiomerically pure [^{18}F]talazoparib as a potential next-generation PARP radiotracer together with a preliminary *in vitro* evaluation and pilot *in vivo* study in mice.

RESULTS AND DISCUSSION

The late-stage radiosynthesis of chiral [^{18}F]talazoparib can be achieved via two possible approaches. The most obvious approach would be to employ an enantiomerically pure precursor in the radiosynthesis. However, for an uncharacterized radiotracer, chiral separation of the precursor would be costly and time-consuming, with a risk of product racemization during the synthesis. We thus decided to pursue an approach that first involves the production and purification of the racemic radiotracer, followed by enantiomeric resolution, isolation, and formulation of the active enantiomer. Therefore, as the radiochemical yield would be reduced by half (assuming a 1:1 ratio of enantiomers), the radiosynthesis would need to be carefully optimized for maximum radiochemical yield to ensure an adequate and reliable synthesis output for biological studies. The two possible sites for late-stage isotopic ^{18}F radiolabeling are both situated on electron-rich or -neutral aromatic rings. This excludes the use of traditional S_NAr radiofluorination in favor of more recently developed methodologies such as CMRF chemistry. However, the proposed radiotracer contains multiple heteroaromatic nitrogen atoms that have been shown to have detrimental effects on CMRF based radiosyntheses.[41] These moieties are thought to complex with the copper-mediator, forming unreactive copper species that inhibit radio-

synthesis performance. For this reason, we set out to develop a protecting group strategy that would allow for maximal radiosynthetic performance while still affording an easily accessible, convenient to use, and shelf-stable precursor.

Chemistry. We adapted the synthesis of the precursor from the synthetic route employed by Wang *et al.* for the synthesis of talazoparib (Scheme 1).[24] 1-methyl-1H-1,2,4-triazole was formylated to **1** via the published procedure.[42] **1** was then condensed with commercially available 6-fluoro-4-nitroisobenzofuran-1(3H)-one in THF in the presence of NEt_3 and Ac_2O to afford **2** in a 53% yield. The resulting lactone **2** was opened to give the keto-ester derivative **3** by warming in methanol with a catalytic amount of acetic acid. In the original synthesis, **3** was then reacted with 4-fluorobenzaldehyde in THF and methanol via reductive cyclization driven by $TiCl_3$ to afford **4b**. This intermediate was then cyclized with hydrazine monohydrate to afford (±)talazoparib (**5b**) as a non-radioactive reference compound. Performing the same two-step procedure with **3** and 4-bromobenzaldehyde afforded the derivatizable bromide **5a**.

Scheme 1: Synthesis of advanced intermediates for [^{18}F]talazoparib precursor synthesis.

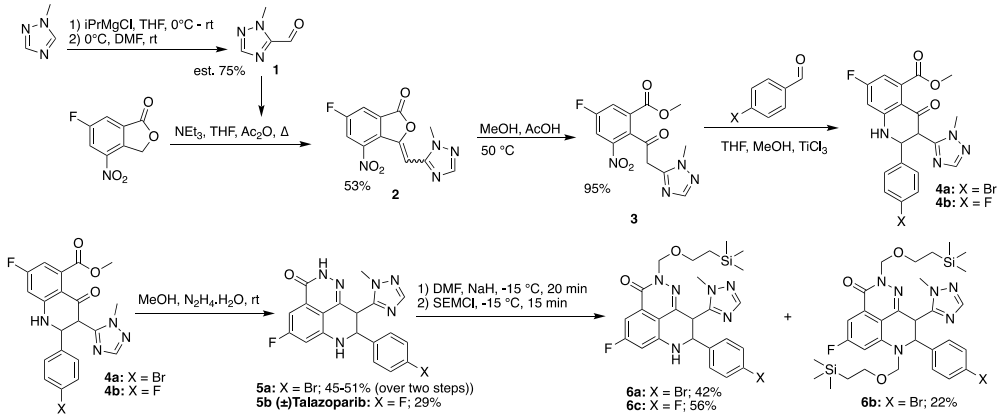

A protecting group strategy using the trimethylsilylethoxymethyl (SEM) ether protecting group was successfully employed by Wilson *et al.* for the "de-risked" radiosynthesis of [^{18}F]olaparib, a PARP tracer structurally related to talazoparib.[40, 43-44] We thus applied the same protecting group strategy to compounds **5a** and **5b**, which were protected with SEM-Cl using sodium hydride in DMF at 0 °C. These conditions afforded both the mono- (**6a**) and di-SEM (**6b**) protected bromide derivatives in an approximate 2:1 ratio. **5b** was exclusively converted to the mono-protected fluoride derivative **6c** for use as a non-radioactive reference compound**.**

Compounds **6a** and **6b** were then further derivatized to yield several potential precursors for radiolabeling. Compounds **6a** and **6b** were converted to their corresponding boronic acid pinacol esters under Miyaura borylation conditions in DMF with KOAc, bis(pinacolato)diboron, and $Pd(dppf)Cl_2$ as the catalyst (Scheme 2). This afforded the compounds **7a** and **7b** in good to excellent yields. **7a** was purified through recrystallization as a shelf-stable and convenient-to-handle white crystalline solid. **7b** was purified through chromatography and was much harder to obtain in the high purities required for reliable radiochemistry. Despite being of high chromatographic purity (HPLC-MS), samples of **7b** displayed a complex NMR spectrum, indicative of multiple conformational isomers. Moreover, **7b** was found to degrade to the more stable **7a** over time. CMRF chemistry has also been well established with aryl stannane precursors, and we have investigated this variation of the CMRF reaction extensively in our previous work.[38] Thus, the analogous stannylation of **6a** was carried out with bis tributyltin to afford the stannyl precursor **7c** as an amorphous glass.

Scheme 2: Synthesis of [^{18}F]talazoparib precursors

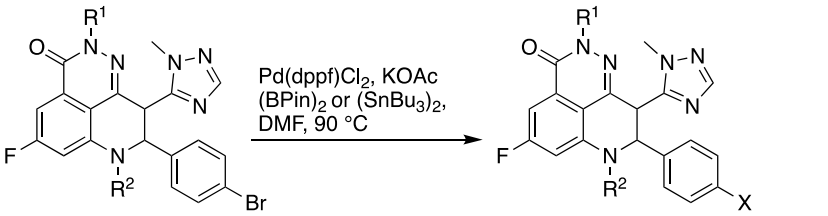

6a: R^1 = SEM, R^2 = H
6c: R^1, R^2 = SEM

7a: X = BPin; R^1 = SEM; R^2 = H; 89%
7b: X = BPin; R^1, R^2 = SEM 34%
7c: X = $SnBu_3$; R^1 = SEM; R^2 = H; 44%

Optimal chiral HPLC conditions were screened using racemic (±)talazoparib (**5b**) in combination with commercially obtained authentic samples of talazoparib and LT-674. CHIRALPAK IA-U, IB-U, IC-U, and IG-U columns (1.6 µm particle diameter, DÄICEL Chiral Technologies, France) were tested for their abilities to resolve the two enantiomers under reversed-phase conditions (water with 0.1% TFA: acetonitrile). CHIRALPAK IB packing material was found to provide good enantiomeric resolution at a relatively low retention time (Figure S7). CHIRALPAK IB-N5 (5 µm) columns run with reversed-phase conditions would thus be used for both semipreparative enantiomeric resolution of [^{18}F]talazoparib and [^{18}F]LT-674, and for chiral radio-HPLC for quality control (QC) analysis.

Radiochemistry and DoE Optimization. With the precursors **7a-c** in hand, we set out to evaluate which precursor would provide the best radiosynthesis performance while still being relatively easy to produce, shelf-stable, and convenient to handle. A series of pilot experiments carried out using each precursor under a small set of arbitrarily chosen unoptimized reaction conditions determined that compounds **7b** and **7c** displayed a marginally better reaction performance (17% and 19% respectively, data not shown) than **7a** (8-15% RCY). As expected, the di-SEM protected derivative **7b** offered the best overall reaction performance under unoptimized conditions; however, as **7a** proved easier to synthesize, purify, and characterize, as well as being shelf-stable, it was chosen as the preferred precursor for further development and optimization.

We have previously explored the use of DoE to solve complex radiochemical optimization problems and have developed an ^{18}F processing method and workflow that is compatible with both small-scale DoE radiochemical experiments and large-scale automated tracer production.[39] We applied this workflow to a computer-generated D-optimal DoE study designed to investigate the effects of precursor load (*Pre*, 5-30 µmol), copper-mediator load (*Cop*, 5-40 µmol), pyridine load (*Py*, 20-500 µmol), and concentration of *n*-BuOH co-solvent (*Bu*, 0-75%) in DMA, on reaction performance (Figure 1, A). The study consisted of 24 experiments (including centerpoints) and was conducted over 5 days (5 runs/day) using [^{18}F]fluoride from cyclotron target washes (Table S1). Each run was carried out for 20 minutes at 120 ℃ before evaluation by radioTLC. Analysis of the data revealed the presence of one outlier (Table S1, exp 21), which was excluded from the final regression model. The remaining data (n = 23) was used to fit a regression model with R^2 = 0.946 (goodness of model fit) and Q^2 = 0.855 (goodness of model prediction), suggesting the model to be valid and predictive (Figure S1).

The use of larger amounts of the precursor was found to positively affect reaction performance, while smaller quantities of the copper mediator ($Cu(OTf)_2$) were beneficial (Figure 1, B). A small amount of *n*-BuOH (5-10%) was also found to provide a small increase in reaction performance. It is thought that *n*-BuOH increases the rate of the CMRF transmetalation step.[45] Factor interactions (where the setting of one factor affects the behavior of another) were found between pyridine and the precursor amount as well as pyridine and *n*-BuOH. The effect of pyridine on reaction performance was found to possess strong quadratic (*Py*Py*, curved) behavior. Optimal reaction conditions of 30 µmol **7a**,

300 µmol pyridine, and 5 µmol $Cu(OTf)_2$ in DMA with 10% *n*-BuOH, were chosen from the response surface plot generated from the regression model (Figure 1, C) These conditions were validated manually using full batches of processed [^{18}F]TBAF and were able to produce protected (±)[^{18}F]**6c** with 57 ± 7.5 %RCY (n = 6) (compound identity was verified using the non-radioactive standard **6c**). These results align with the DoE model and afford the product in yields acceptable for establishment as an automated radiosynthesis featuring enantiomeric resolution. Quantitative deprotection to (±)[^{18}F]talazoparib (>95% conversion according to HPLC) was achieved with 6 M HCl at 120 ℃ for 15 minutes (compound identity was verified against the non-radioactive standard **5b**).

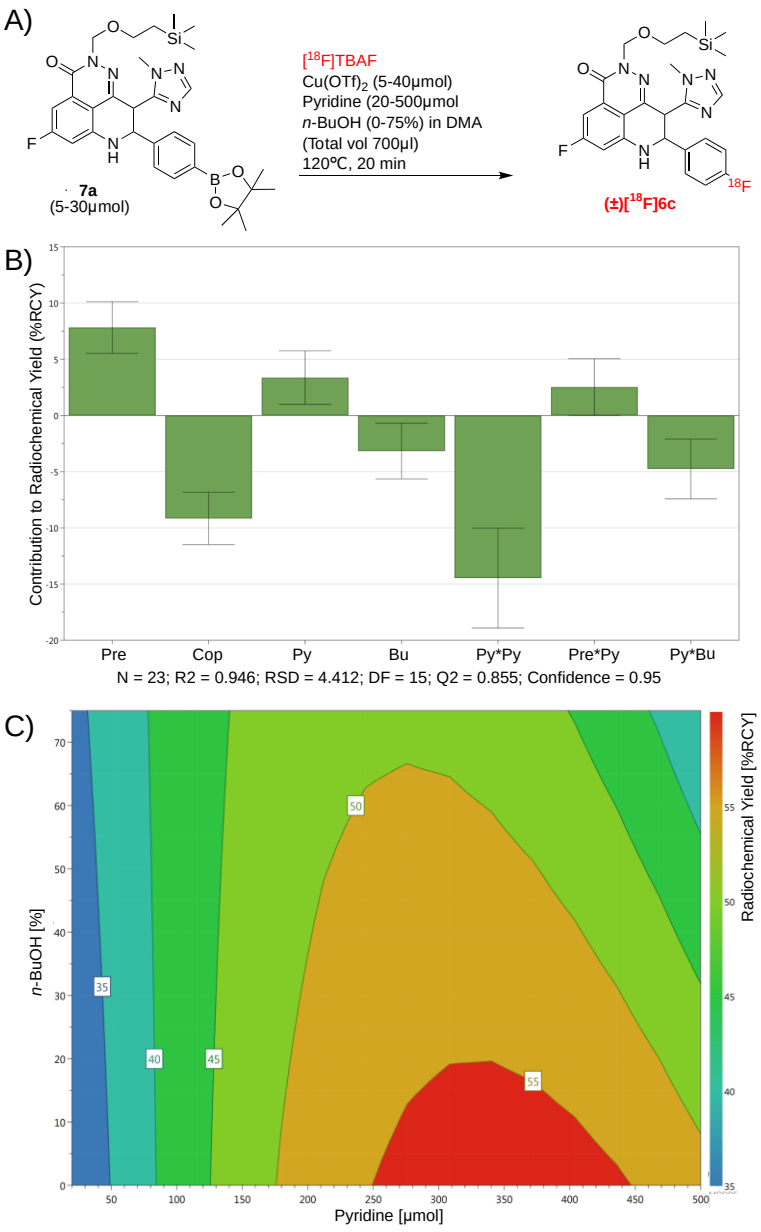

Figure 1: A) A D-optimal DoE study was used to optimize the radiolabeling of **7a**. B) The scaled and centered regression coefficient calculated from the results of the D-optimal response surface modeling study of the radiosynthesis of [^{18}F]**6c**. Large bars represent factors with a large contribution to the response (%RCY). A positive number denotes a

positive influence on the response. A negative number indicates a diminishing effect on the response. If a factor's regression coefficient is smaller than the associated error bars, it is probable (at the 95% confidence interval) then that factor is not significant. C) A section of the response surface calculated from the regression model. Variables not shown: *Cop* = 5 µmol, *Pre* = 30 µmol (see Figure S3 for the entire 4D response surface plot.)

Automated Radiochemistry. The optimized CMRF radiosynthesis was translated onto two different synthesis platforms: An Elixys Flex/Chem automated radiosynthesizer coupled to a Pure/Form purification and formulation module (Sofie Biosciences, USA) and an FX N Pro (GE Healthcare, Sweden). The Elixys Flex/Chem platform is a cassette-based system (up to 3 reactors) and can perform complex multi-reactor radiosyntheses. The Pure/Form module is equipped with two semipreparative HPLC injection loops (5 ml each) and up to 3 selectable HPLC columns. Therefore, this setup would allow for the sequential HPLC-based purification and enantiomeric resolution required for the synthesis of [^{18}F]talazoparib. The Tracerlab FX N Pro is a fixed fluid path system with a single HPLC injection loop and column. The purified product racemate must, therefore, be transferred to a secondary external HPLC system (in this case, an Elixys Pure/Form) for enantiomeric resolution. While the exact technical details differ between the two synthesis modules (the radiosynthesis using both systems are described in detail in the Supplementary Information), the automated synthesis of [^{18}F]talazoparib follows the same general procedure irrespective of which module is used (Figure 2).

The DoE optimized reaction mixture was added to the processed [^{18}F]TBAF and reacted at 120 °C for 20 minutes. This was followed by the removal of the SEM protecting group with 6 M HCl at 120 °C for 15 minutes. The pH of the reaction mixture was then adjusted to pH 5-7 with the addition of ammonium formate solution (25 mM, 5-10 ml, dependent on the automated system used) containing NaOH (6 M, 600 µl). The diluted reaction mixture was passed over an HLB SPE cartridge (Waters, USA), trapping the product (±)[^{18}F]talazoparib and removing the DMA, residual salts, and unreacted [^{18}F]fluoride. While some product is lost, especially when lower dilution volumes are used, this step is important to ensure efficient HPLC purification. The product was then eluted from the HLB cartridge with acetonitrile (1 ml) and reformulated with HPLC buffer (4 ml) for injection onto the first HPLC column. The reaction mixture was then subjected to purification via C18 reversed-phase HPLC to separate the product racemate from the remaining precursor and other CMRF reaction byproducts. The product HPLC peak was isolated (≈ 5 ml) and this solution was then transferred to a second HPLC injection loop for enantiomeric resolution using a semipreparative CHIRALPAK IB-N5 (5µm, 10 × 250 mm) column operating under reversed-phase conditions. The desired enantiomer, either [^{18}F]talazoparib or [^{18}F]LT-674, was then isolated, diluted, and trapped on a second HLB cartridge. The product was then eluted from the cartridge and formulated for injection with ethanol and phosphate-buffered saline (PBS, final ethanol content 5%). This procedure yielded enantiomerically pure (>99% ee) [^{18}F]talazoparib (or [^{18}F]LT-674) with 13 ± 3.4% RCY (n = 4) (radioactivity yield (%AY) = 4 – 8% over 120 minutes; molar radioactivity = 52 – 176 GBq/µmol). Product identity, chemical and radiochemical purity, and molar activity were determined using CHIRALPAK IB-N5 (5 µm, 4.6 × 150 mm) analytical HPLC against the commercially available non-radioactive standard compounds. This synthesis produced both [^{18}F]talazoparib and [^{18}F]LT-674 in good yields, chemical and radiochemical purities, and molar activities for both *in vitro* and *in vivo* preclinical evaluation.

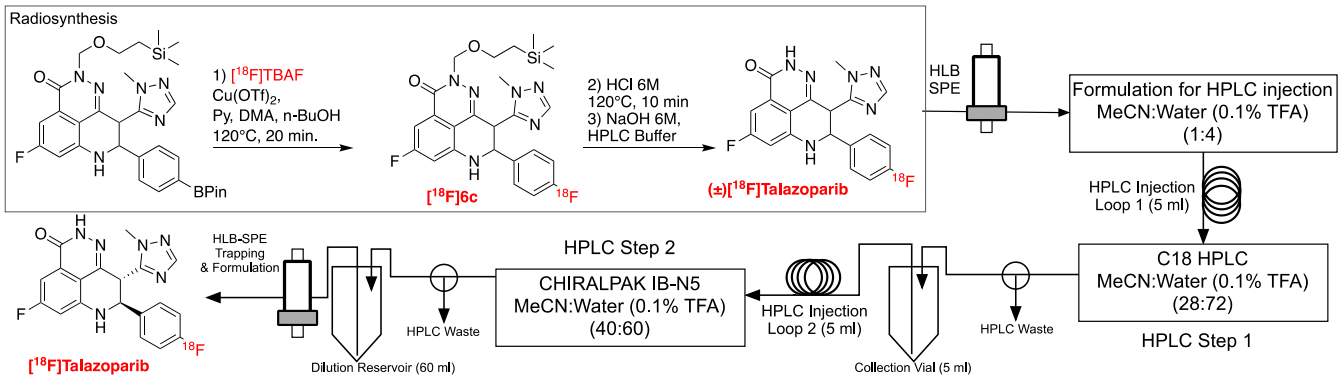

Figure 2: The general automated procedure for the radiosynthesis, HLB-SPE clean-up, 2D HPLC purification and chiral resolution, and product concentration and formulation of [^{18}F]talazoparib.

***In Vitro* Evaluation.** [^{18}F]talazoparib demonstrated high uptake in human breast cancer cells (HCC1937), while, as expected, the inactive enantiomer [^{18}F]LT-674 showed only very low radiotracer uptake (Figure 3). [^{18}F]Talazoparib signal was blockable to baseline with excesses of both olaparib and talazoparib. Olaparib was found to be less effective at blocking [^{18}F]talazoparib signal than talazoparib. This effect was confirmed using a concentration-dependent blocking assay, revealing IC_{50} values of 14.51 and 23.77 nM for talazoparib and olaparib, respectively (Figure S14). As talazoparib blocked the amount of bound [^{18}F]talazoparib to a significantly greater extent than olaparib, we theorize that this difference represents talazoparib's ability to bind a wider array of other PARP isoforms, an effect that we plan to investigate further.[22, 46]

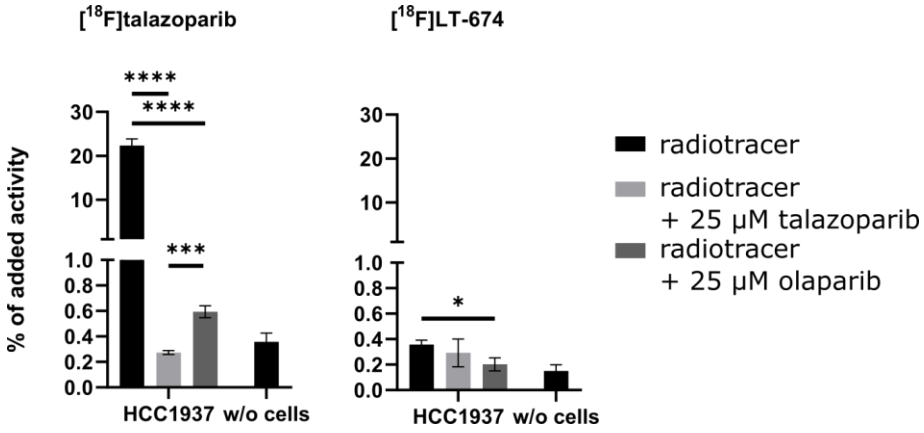

Figure 3: Uptake of [^{18}F]talazoparib (left) and the inactive enantiomer [^{18}F]LT-674 (right) in HCC1937 cells, blocked with olaparib or talazoparib.

***In Vivo* Evaluation.** [^{18}F]Talazoparib was further characterized *in vivo* in HCC1937 xenograft-bearing mice. The stability of [^{18}F]talazoparib was evaluated in mouse and human serum before the *in vivo* experiments, and the radiotracer was found to be stable over a time course of 240 minutes (Figure S17). PET imaging showed substantial tracer uptake in the abdominal tissues as well as in bone and muscle (Figure 4, A), data that are in line with the literature published blockable uptake of other established PARP radiotracers in these organs.[47] These findings were further confirmed by *ex vivo* biodistribution analysis after 2.5 hours post-injection (p.i.)(Figure 4, B). PARP1 expression in the xenograft tissue was verified *ex vivo* by PARP1 immunofluorescence microscopy (Figure S16).

[^{18}F]Talazoparib showed an elevated uptake in the tumor xenografts at 1 hour p.i. relative to reference tissues. The specific uptake was found to further intensify up to the 2-hour p.i. timepoint. *Ex vivo* biodistribution data showed the absolute xenograft uptake to be 3.7 ± 0.7 %ID/g with a mean tumor-to-muscle ratio (TMR) of 1.8 ± 0.4 (Figure 4, C). The TMR was comparable to the reported TMR (1.9, 60 minutes p.i.) of the PARP tracer [^{18}F]FTT in the same xenograft model.[30] The tumor-to-blood ratio (TBR) of [^{18}F]talazoparib is exceptionally high (10.2 ± 1.5) and exceeds the TMR by a factor of 5.6. In the context of our *in vitro* data, we hypothesize that the high muscle uptake observed in this animal model may be caused by the binding of [^{18}F]talazoparib to other PARP enzymes or an as-of-yet unidentified protein target. These questions will be the subject of future investigations using this novel radiotracer.

[^{18}F]Talazoparib exhibited balanced clearance between both renal and hepatobiliary pathways with a mean liver-to-kidney ratio (LKR) of 1.1 ± 0.1, a finding which was confirmed by the time-activity curves (TAC) obtained from dynamic PET imaging (Figure S15). While no tracer uptake was observed in the *ex vivo* biodistribution data, the brain TAC shows an initial perfusion peak with complete tracer washout occurring rapidly thereafter. Thus, [^{18}F]talazoparib uptake could be examined in glioblastoma models, a setting in which the observed high muscle uptake would only play a minor role. Fast blood clearance with a calculated blood half-life of 3.3 minutes was determined.

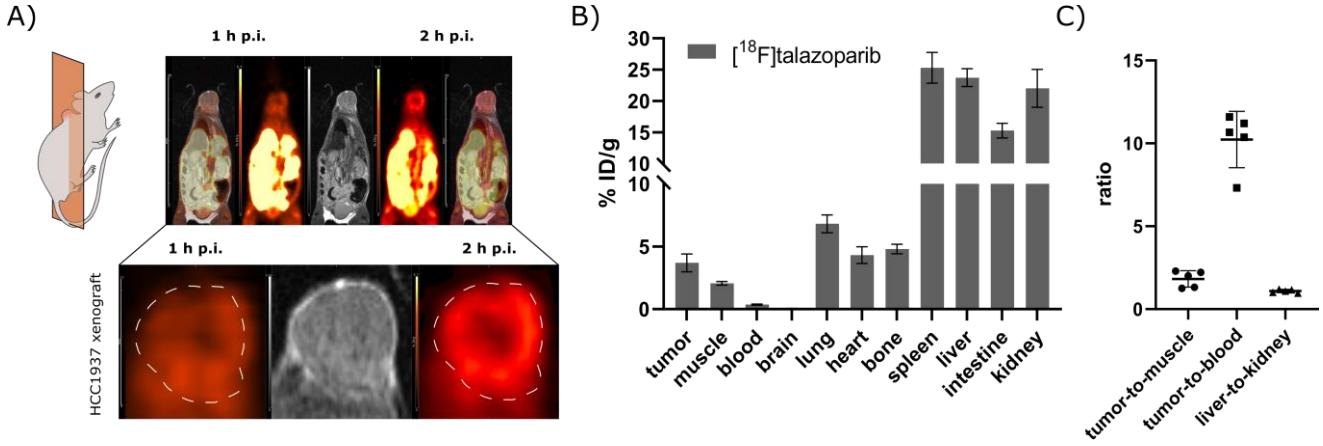

Figure 4: A) Representative PET images of one mouse 1 hour p.i. (left, last 10 minutes of a 1-hour dynamic scan) and 2 hours p.i. (right, 10-minute static scan) with the corresponding MR image. The respective xenograft is displayed enlarged underneath. B) Biodistribution of [^{18}F]talazoparib in various organs 2.5 hours p.i. (n = 5). C) TMR, TBR, and LKR of mice injected with [^{18}F]talazoparib (n = 5) 2.5 hours p.i.

CONCLUSIONS

Fluorine is present in many clinically relevant drug-like molecules that may serve as candidates for novel imaging probes. PET imaging is also becoming more important as a valuable research tool to assess the *in vivo* pharmacological properties of promising drug candidates in real-time. The synthesis and evaluation of enantiomerically pure [^{18}F]talazoparib discussed here serves as an example of how an efficient DoE based tracer development pipeline can be used to aid in the establishment of procedurally complex ^{18}F based radiosyntheses. Given the time constraints of ^{18}F radiochemistry, our decision to perform enantiomeric resolution after the radiolabeling step meant that our synthesis needed to be optimized for radiochemical efficiency from the outset. Using information from previous radiosynthesis “de-risking” studies[40, 43-44], we were able to rapidly identify and test a suitable protecting group strategy and identify a focused set of precursor candidates. After selecting a precursor that was shelf-stable, easy to obtain, and handle, although not necessarily chemically optimal, we used DoE to discover a set of reaction conditions that would produce

(±)[^{18}F]talazoparib in yields sufficient for enantiomeric resolution, product formulation, and subsequent delivery for preclinical evaluation.

While [^{18}F]talazoparib was found to target PARP1 expression in an established tumor model effectively, the *in vitro* and *in vivo* results of this work highlight the importance of the further exploration of [^{18}F]talazoparib as a PARP imaging agent for alternative indications. In particular, the use of [^{18}F]talazoparib to quantify PARP isoforms beyond PARP1/2 may be of clinical merit. [^{18}F]Talazoparib may thus allow us to study the PARP family of proteins from a new angle.

EXPERIMENTAL

General. All chemicals, reagents, catalysts, and solvents were purchased from either Sigma Aldrich (Steinheim, Germany), Merck (Darmstadt, Germany), abcr GmbH (Karlsruhe, Germany), Carl Roth (Karlsruhe, Germany), and were used without any additional purification unless otherwise stated. QMA, SPE, and SEP-PAK cartridges were obtained from Waters (Milford, Massachusetts, USA) unless otherwise stated. Reactions were monitored using thin-layer chromatography (TLC) on 0.20 mm Polygram SIL G/UV$_{254}$ (silica gel 60) TLC plates and were developed with an appropriate running buffer/solvent mixture. Spots were visualized with UV light (254 or 366 nm). Preparative flash chromatography was performed using pre-packed silica gel columns (SNAP KP-Sil or SNAP Ultra (25 µm HP-Sphere), 10 g, 25 g, 50 g, or 100 g, (Biotage, Uppsala, Sweden)) on an automated chromatography system (Isolera 4, Biotage) which featured a UV detector and fraction collector. Unless otherwise stated, all columns were dry loaded by absorption onto either silica gel or diatomaceous earth packing material (Isolute, Biotage). ^{1}H and ^{13}C NMR spectra were obtained at 300 K using an Avance III AV 600 (^{1}H: 600.13 MHz and ^{13}C: 150.61 MHz) spectrometer (Bruker Biospin, Ettlingen, Germany). All chemical shifts (δ) are reported in ppm, and all *J* values are reported in Hz. The following abbreviations are used to describe multiplicities: s (singlet), d (doublet), t (triplet), q (quartet), m (multiplet) brs (broad singlet). All compounds were dissolved in chloroform ($CDCl_3$) unless otherwise stated. All chemical shifts were referenced to residual chloroform (δ_H = 7.24 and δ_C = 77.00) or DMSO (δ_H = 2.50 and δ_C = 39.52). Analytical HPLC-MS data was collected using a 1200 series HPLC machine coupled to quadrupole 6120 series MS detector in ESI mode (Agilent, Santa Clara, California, USA) under the following conditions: Column: Luna 5 µm C18 (2) 100 Å, 50 x 2 mm; Solvent A: H_2O + formic acid (0.1%); Solvent B: acetonitrile; Gradient: 0-7.60 min (0% - 100% B), 7.60 - 7.80 min (100% B), 7.80 - 8.30 min (100% - 0% B), 8.30 - 12.0 min (0% B). High-resolution mass spectroscopy (HRMS) was acquired using a maXis4G mass spectrometer (Bruker Daltonics, Bremen, Germany) operating using electron spray ionization time-of-flight. (ESI-TOF). Deviation from the calculated mass was found to be < 2 .00 ppm for all measured compounds.

Chemical synthesis. 1-*Methyl-1H-1,2,4-triazole-5-carbaldehyde (*1*).* 1-methyl-1H-1,2,4-triazole (10 g, 120 mmol) was dissolved in THF (60 ml) in a dry argon purged two-neck reaction flask fitted with a rubber septum, and the resulting solution was then cooled to 0 °C. A solution of 2 M isopropyl magnesium chloride (66 ml, 132 mmol) was then added dropwise through the septum via a syringe over 15 min. The reaction mixture was then allowed to warm slowly to room temperature and stir for 1.5 hours. The reaction vessel was again cooled to 0 °C, after which N,N-dimethyl formamide (DMF) (14 ml, 180.5 mmol) was added dropwise via syringe. The reaction mixture was once more allowed to slowly warm to room temperature and stir overnight. The next morning, the reaction was quenched by the slow addition of HCl (2 M) until pH 2, and the resulting mixture was diluted with DCM (100 ml). The phases were separated with a separating funnel, and the aqueous phase was neutralized with saturated aqueous sodium bicarbonate ($NaHCO_3$) and extracted with DCM (2 x 80 ml). The organic fractions were combined, washed once with brine, dried with magnesium sulfate (MgSO4), and concentrated under reduced pressure to remove the DCM. Product **1** is a volatile oil (≈60 °C) and was thus not purified further. The compound was used, in excess, directly in the next step without further analysis, assuming a synthesis yield of 75% (presented in previous literature).[42]

*6-Fluoro-3-((1-methyl-1H-1,2,4-triazol-5-yl)methylene)-4-nitroisobenzofuran-1(3H)-one (**2**).* Commercially available 6-fluoro-4-nitroisobenzofuran-1(3*H*)-one (9.8 g, 50 mmol), a solution of **1** in THF (ca. 100 mmol, assuming 75% conversion in

the previous step), and triethylamine (21 ml, 150 mmol) were dissolved in dry THF (150 ml) in an argon-filled two-neck reaction flask fitted with a reflux condenser. Acetic anhydride (35 ml) was then added dropwise to the reaction mixture over 3 min, and the resulting mixture was then heated to reflux for 1 hour. The mixture was then removed from the heat and concentrated under reduced pressure to a volume of approximately (10 ml) until a green/yellow precipitate formed. The resulting slurry was then cooled in a freezer to -5 °C, and the solid was collected through vacuum filtration. The resulting cake was washed with cold ethyl acetate, and the residue was then dried under high vacuum for 4 hours to afford **2** as a grey-green solid (7.34 g, 50 %). The analytical data are in agreement with the literature.[24]

^{1}H NMR (600 MHz, DMSO): δ 7.74 (dd, *J* = 8.7, 2.3 Hz, 1H, Ar), 7.56 (dd, *J* = 6.4, 2.4 Hz, 1H, Ar), 7.25 (s, 1H, TzH), 6.32 (s, 1H, C=CH), 3.09 (s, 3H, Me).

*Methyl 5-fluoro-2-(2-(1-methyl-1H-1,2,4-triazol-5-yl)acetyl)-3-nitrobenzoate (**3**)*. Compound 2 (7.34 g, 25.2 mmol) was suspended in methanol (204 ml), and acetic acid (0.5 ml) was added to the resulting solution. The mixture was then warmed to 50 °C until HPLC-MS confirmed complete consumption of the starting material (4 – 12 hours). The solvents were then removed under high vacuum to afford 3 as a yellow solid in nearly a quantitative yield (8.1 g, 99%). The product was used directly in the next step without further purification. The analytical data are in agreement with the literature.[24] ^{1}H NMR (600 MHz, DMSO): δ 8.52 (dd, *J* = 8.2, 2.6 Hz, 1H, Ar), 8.26 (dd, *J* = 8.3, 2.6 Hz, 1H, Ar), 7.85 (s, 1H, TzH), 4.59 (s, 2H, CH_2), 3.91 (s, 3H, Me), 3.88 (s, 3H, Me); ^{13}C NMR (151 MHz, DMSO) δ 195.48, 163.48, 161.21 (d, *J* = 252.6 Hz), 150.18, 148.75, 147.10 (d, *J* = 8.8 Hz), 133.58, 131.24 (d, *J* = 7.7 Hz), 123.63, 117.09 (d, *J* = 26.9 Hz), 53.71, 40.55, 35.34.

*8-(4-Bromophenyl)-5-fluoro-9-(1-methyl-1H-1,2,4-triazol-5-yl)-2,7,8,9-tetrahydro-3H-pyrido[4,3,2-de]phthalazin-3-one (**5a**) and 5-fluoro-8-(4-fluorophenyl)-9-(1-methyl-1H-1,2,4-triazol-5-yl)-2,7,8,9-tetrahydro-3H-pyrido[4,3,2-de]phthalazin-3-one (**5b**).*

5a: Compound **3** (8.1 g, 25.2 mmol) and 4-bromobenzaldehyde (8.9 g, 50.5 mmol) were suspended in THF (50 ml) and MeOH (10 ml). To the resulting mixture was added titanium (III) chloride solution (20% wt solution in HCl (2 M), 130 ml, 6 Eq.) in dropwise fashion over 30 min at room temperature. The reaction temperature was maintained between 30 and 50 °C for 2 hours, after which it was quenched by the slow addition of water (260 ml). The reaction mixture was then poured into a separating funnel and extracted with ethyl acetate (4 x 140 ml). The organic fractions were pooled and washed with $NaHCO_3$ (3 x 60 ml) and $NaHSO_3$ (3 x 100 ml), dried with sodium sulfate (Na_2SO_4), and concentrated under reduced pressure to afford a think yellow syrup, which was carefully washed with aliquots of diethyl ether (3 x 10 ml). The resulting yellow syrup was then dried under high vacuum to afford the crude intermediate **4** as a yellow amorphous solid (11.3 g, 98%) that was used in the next step without any further purification.

Intermediate **4** (11.3 g, 24.6 mmol) was dissolved in methanol (30 ml) at room temperature, and to the resulting solution was added hydrazine monohydrate (7.7 ml). The reaction mixture was then left to stir overnight at room temperature. The next morning the resulting white precipitate was collected via vacuum filtration to afford Compound **5** as an off-white solid (4.9 g, 45% over two steps).

5a: ^{1}H NMR (600 MHz, DMSO): δ 12.35 (s, 1H, NH), 7.81 (s, 1H, TzH), 7.72 (s, 1H, NH), 7.55 – 7.50 (m, 2H, Ar), 7.43 – 7.39 (m, 2H, Ar), 7.07 (dd, *J* = 9.0, 2.4 Hz, 1H, Ar), 6.91 (dd, *J* = 11.1, 2.5 Hz, 1H, Ar), 5.00 (m, 2H, CH, CH), 3.68 (s, 3H, Me); ^{13}C NMR (151 MHz, DMSO): δ 165.40 (d, *J* = 248.2 Hz), 159.37 (d, *J* = 3.5 Hz), 152.36, 150.77, 148.78 (t, *J* = 12.7 Hz), 141.38, 139.03, 131.77, 130.74, 130.35 (d, *J* = 11.1 Hz), 121.96, 111.76, 103.33 (d, *J* = 26.7 Hz), 99.08 (d, *J* = 24.7 Hz), 59.14, 42.85, 35.40; HRMS (ESI): m/z calcd for $C_{19}H_{15}BrFN_6O$ $[M+H]^+$, 441.04693; found, 441.04736.

5b: To synthesis **5b,** the same general procedure was followed using compound **3** (800 mg, 2.5 mmol), 4-flurobenzaldehyde (462 mg, 3.7 mmol), and titanium (III) chloride solution (20% wt solution in HCl (2 M), 9.4 ml, 6 Eq.). The resulting intermediate **4b** was treated with hydrazine monohydrate (1.5 ml) to afford **5b** (274 mg, 29%). Spectral analysis agreed with the published data.[24] **5b talazoparib**: ^{1}H NMR (600 MHz, DMSO): δ 12.35 (s, 1H, NH), 7.81 (s, 1H, TzH), 7.73 (s, 1H, NH), 7.52 – 7.47 (m, 2H, Ar), 7.20 – 7.13 (m, 2H, Ar), 7.08 (dd, *J* = 8.9, 2.5 Hz, 1H, Ar), 6.93 (dd, *J* = 11.2, 2.5 Hz, 1H, Ar), 5.01 (m, 2H, CH, CH), 3.67 (s, 3H, Me).

*8-(4-Bromophenyl)-5-fluoro-9-(1-methyl-1H-1,2,4-triazol-5-yl)-2-((2-(trimethylsilyl)ethoxy)methyl)-2,7,8,9-tetrahydro-3H-pyrido[4,3,2-de]phthalazin-3-one (**6a**), 8-(4-Bromophenyl)-5-fluoro-9-(1-methyl-1H-1,2,4-triazol-5-yl)-2,7-bis((2-(trimethylsilyl)ethoxy)methyl)-2,7,8,9-tetrahydro-3H-pyrido[4,3,2-de]phthalazin-3-one (**6b**), and 5-fluoro-8-(4-fluorophenyl)-9-(1-methyl-1H-1,2,4-triazol-5-yl)-2-((2-(trimethylsilyl)ethoxy) methyl)-2,7,8,9-tetrahydro-3H-pyrido[4,3,2-de]phthalazin-3-one (**6c**).*

6a and **6b**: Sodium hydride (60% in mineral oil, 181 mg, 4.53 mmol) was suspended in DMF (10 ml) in a dry, argon-filled flask, and the resulting solution was then cooled to 0 °C. Compound **5a** (1 g, 2.27 mmol) was added to the NaH suspension in small portions, and DMF (2 ml) was used to wash any compound off the vessel walls. The deep red/purple solution was allowed to stir for 15 minutes, whereupon a solution of (trimethylsilyl)ethoxymethyl chloride (752 mg, 4.53 mmol) in DMF (2 ml) was added dropwise through a rubber septum over 5 minutes. Throughout the addition, the solution turned clear and light orange and was allowed to stir for a further 20 min before being quenched with sat. Aq. NH_4Cl (10 ml). The reaction mixture was diluted with water (250 ml) and transferred to a separating funnel, where it was extracted with ethyl acetate (3 x 50 ml). The organic fractions were pooled, dried with $MgSO_4$, and evaporated to dryness. The crude product residue was then purified using flash chromatography (40% EtOAc in hexanes) to afford compounds **6a** and **6b** as crystalline solids (**6a**: 547 mg, 42 %; **6b**: 347 mg, 22%). Despite the presence of several minor impurities both compounds were used in the next step without further purification. **6a**: ^{1}H NMR (600 MHz, $CDCl_3$): δ 7.80 (s, 1H, TzH), 7.39 (d, *J* = 8.5 Hz, 2H, Ar), 7.32 (dd, *J* = 8.5, 2.3 Hz, 1H, Ar), 7.24 (d, *J* = 8.5 Hz, 2H, Ar), 6.75 (dd, *J* = 10.0, 2.3 Hz, 1H, Ar), 5.36 (d, J_{gem} = 9.9 Hz, 1H, CH_2), 5.31 (s, 1H, NH), 5.21 (d, J_{gem} = 9.9 Hz, 1H, CH_2), 5.13 (d, *J* = 11.1 Hz, 1H, CH), 4.43 (d, *J* = 11.0 Hz, 1H, CH), 3.64 (s, 3H, Me), 3.60 – 3.48 (m, 2H, CH_2), 0.90 – 0.81 (m, 2H, CH_2), -0.06 (s, 9H); ^{13}C NMR (151 MHz, $CDCl_3$): δ 167.05 (d, *J* = 253.1 Hz), 160.49 (d, *J* = 3.4 Hz), 152.80, 151.64, 148.17 (d, *J* = 11.8 Hz), 141.07, 139.07, 133.46, 131.69 (d, *J* = 11.0 Hz), 130.55, 124.42, 112.90, 105.77 (d, *J* = 26.8 Hz), 104.08 (d, *J* = 24.6 Hz), 80.91, 68.78, 61.15, 46.06, 36.69, 19.46, 0.00; HRMS (ESI): m/z calcd for $C_{25}H_{28}BrFN_6O_2SiNa$ $[M+Na]^+$, 593.11026; found, 593.11030.

6b: ^{1}H NMR (600 MHz, $CDCl_3$): δ 7.72 (s, 1H, TzH), 7.43 (dd, *J* = 8.5, 2.3 Hz, 1H, Ar), 7.39 (d, *J* = 8.5 Hz, 2H, Arj), 7.10 (dd, *J* = 11.4, 2.3 Hz, 1H, Ar), 7.07 (d, *J* = 8.5 Hz, 2H, Ar), 5.40 (d, *J* = 9.9 Hz, 1H, CH_2), 5.36 (d, *J* = 9.9 Hz, 1H, CH_2'), 5.21 (d, *J* = 3.9 Hz, 1H, CH), 4.87 (d, *J* = 11.2 Hz, 1H, CH_2), 4.78 (d, *J* = 11.2 Hz, 1H, CH_2'), 4.53 (d, *J* = 3.9 Hz, 1H, CH), 3.93 (s, 3H, Me), 3.61 – 3.56 (m, 2H, CH_2), 3.45 – 3.38 (m, 1H, CH_2), 3.38 – 3.21 (m, 1H, CH_2'), 0.90 – 0.78 (m, 4H, CH_2), -0.08 (s, 9H, $SiMe_3$), -0.09 (s, 9H, $SiMe_3$); ^{13}C NMR (151 MHz, $CDCl_3$): δ 167.80 (d, *J* = 252.9 Hz), 160.77 (d, *J* = 3.6 Hz), 154.13, 151.87, 147.34 (d, *J* = 11.8 Hz), 139.40, 139.11, 133.67, 131.67 (d, *J* = 11.8 Hz), 129.99, 123.86, 113.46, 105.98 (d, *J* = 28.2 Hz), 104.17 (d, *J* = 24.6 Hz), 84.26, 80.44, 68.72, 67.45, 66.12, 44.67, 37.61, 19.49, 19.44, 0.00; HRMS (ESI): m/z calcd for $C_{31}H_{42}BrFN_6O_3Si_2Na$ $[M+Na]^+$, 723.19165; found, 723.19109.

6c: The same general procedure was followed using compound **5b** (200 mg, 0.53 mmol), sodium hydride (60% in mineral oil, 46 mg, 1.16 mmol), (trimethylsilyl)ethoxymethyl chloride (192 mg, 1.16 mmol) in DMF (4 ml). These conditions afforded the non-radioactive reference compound **6c** (139 mg, 52%). ^{1}H NMR (600 MHz, $CDCl_3$): δ 7.86 (s, 1H, TzH), 7.45 – 7.37 (m, 3H, Ar), 7.02 (t, *J* = 8.5 Hz, 2H, Ar), 6.80 (dd, *J* = 10.0, 2.3 Hz, 1H, Ar), 5.42 (d, J_{gem} = 9.9 Hz, 1H, CH_2), 5.28 (d, J_{gem} = 9.9 Hz, 1H, CH_2'), 5.28 (s, 1H, NH), 5.20 (d, *J* = 11.1 Hz, 1H, CH), 4.50 (d, *J* = 11.1 Hz, 1H, CH), 3.68 (s, 3H, Me), 3.67 – 3.56 (m, 2H, CH_2), 0.95 – 0.86 (m, 2H, CH_2), 0.00 (s, 9H, $SiMe_3$); ^{13}C NMR (151 MHz, $CDCl_3$): δ 167.07 (d, *J* = 253.0 Hz), 164.22 (d, *J* = 248.8 Hz), 160.51 (d, *J* = 3.5 Hz), 152.90 (, 151.58, 148.21 (d, *J* = 11.7 Hz), 141.18, 135.79 (d, *J* = 3.2 Hz), 131.75 (d, *J* = 11.1 Hz), 130.63 (d, *J* = 8.2 Hz), 117.33 (d, *J* = 21.5 Hz), 112.96, 105.70 (d, *J* = 26.9 Hz), 104.11 (d, *J* = 24.5 Hz), 80.90, 68.79, 61.12, 46.33, 36.66, 31.09, 19.47, 15.52; HRMS (ESI): m/z calcd for $C_{25}H_{28}F_2N_6O_2SiNa$ $[M+Na]^+$, 533.19033; found, 533.19021.

*General procedure for the synthesis of compounds **7a-c***: The corresponding bromide (**6a** or **6b**), bis(pinacolato)diboron (2.2 eq), and potassium acetate (3 eq) were suspended in DMF) in a dry argon filled reaction flask fitted with a reflux condenser. [1,1′-bis(diphenylphosphino)ferrocene]dichloropalladium(II) ($Pd(dppf)Cl_2$, 20 mol%) was added to the reaction mixture, and a small portion of DMF was used to wash the catalyst of the vessel walls. The reaction flask was purged with argon, and the reaction was heated to 90 °C for 2-6 hours until HPLC-MS showed conversion of the starting material into the de-

sired product. The reaction mixture was diluted with ethyl acetate (80 ml) and passed through a tightly packed plug of Celite® under vacuum. The filtrate was collected and transferred to a separating funnel, where it was washed with water (200 ml). The aqueous layer was further extracted with ethyl acetate (3 x 80 ml), after which the organic fractions were pooled, washed with brine, dried with MgSO4, and concentrated under reduced pressure to afford the desired product racemate.

*5-fluoro-9-(1-methyl-1H-1,2,4-triazol-5-yl)-8-(4-(4,4,5,5-tetramethyl-1,3,2-dioxaborolan-2-yl)phenyl)-2-((2-(trimethylsilyl)ethoxy)methyl)-2,7,8,9-tetrahydro-3H-pyrido[4,3,2-de]phthalazin-3-one (**7a**)*: The general procedure described above was applied using Compound **6a** (1.448 g, 2.534 mmol), bis(pinacolato)diboron (1.415 g, 5.574 mmol), potassium acetate (746 mg, 7.602 mmol), and $Pd(dppf)Cl_2$ (371 mg, 0.507 mmol, 20 mol%) in DMF (22 ml + 3 ml wash). After 4 hours, these conditions afforded the desired product racemate (**7a**) as an off-white solid (1.391 g, 89%). For radiochemical experiments, the product (515 mg) was further purified by recrystallization. The product was dissolved completely in a hot mixture of acetone and acetonitrile (1:1), and deionized water was then added dropwise until the solution became turbid. The solution was again lightly heated until the solution was nearly transparent, and it was then allowed to slowly cool to the ambient temperature, after which the recrystallization vessel was placed in a refrigerator at 4 °C and allowed to sit overnight. The next day the pure product was collected via vacuum filtration to afford a pure racemic mixture of 7a as a white crystalline solid (361 mg, 70% recovery). ^{1}H NMR (600 MHz, $CDCl_3$): δ 7.78 (s, 1H, TzH), 7.69 (d, *J* = 7.8 Hz, 2H, Ar), 7.34 (dd, *J* = 8.8, 2.3 Hz, 1H, Ar), 7.30 (d, *J* = 7.8 Hz, 2H, Ar), 6.72 (dd, *J* = 10.0, 2.3 Hz, 1H, Ar), 5.37 (d, J_{gem} = 9.9 Hz, 1H, CH_2), 5.28 (s, 1H, NH), 5.22 (d, J_{Gem} = 9.9 Hz, 1H), 5.06 (d, *J* = 11.1 Hz, 1H, CH), 4.47 (d, *J* = 11.1 Hz, 1H, CH), 3.62 – 3.50 (m, 5H, CH, Me), 1.31 (s, 12H, BPin), 0.85 (dd, *J* = 9.1, 7.5 Hz, 2H, CH_2), 0.06 (s, 9H, $SiMe_3$); ^{13}C NMR (151 MHz, $CDCl_3$): δ 167.07 (d, *J* = 252.7 Hz), 160.58 (t, *J* = 3.5 Hz), 153.04, 151.67, 148.31 (d, *J* = 11.8 Hz), 142.85, 141.35, 136.73, 131.74 (d, *J* = 11.0 Hz), 128.07, 112.97, 105.60 (d, *J* = 26.5 Hz), 103.93 (q, *J* = 24.6 Hz), 85.47, 80.86, 68.74, 61.94, 46.06, 36.55, 26.26 (d, *J* = 4.9 Hz), 19.45, 0.00; HRMS (ESI): m/z calcd for $C_{31}H_{40}BFN_6O_4SiNa$ $[M+Na]^+$, 641.28554; found, 641.28497.

*5-fluoro-9-(1-methyl-1H-1,2,4-triazol-5-yl)-8-(4-(4,4,5,5-tetra-methyl-1,3,2-dioxaborolan-2-yl)phenyl)-2,7-bis((2-(trimethylsilyl) ethoxy)methyl)-2,7,8,9-tetrahydro-3H-pyrido[4,3,2-de]phthalazin-3-one (**7b**)*. The same general procedure was used to synthesize compound **7b** using compound **6b** (253 mg, 0.36 mmol), bis(pinacolato)diboron (201 mg, 0.79 mmol), potassium acetate (106 mg, 1.08 mmol), and $Pd(dppf)Cl_2$ (52 mg, 0.07 mmol, 20 mol%) in DMF (4 ml + 1 ml wash). The reaction was stirred at 90 ℃ for 2 hours. This afforded the desired product as an off yellow solid (92 mg, 34%). ^{1}H NMR showed a complex spectrum which suggested the presence of conformational isomers (denoted *):^{1}H NMR (600 MHz, $CDCl_3$): δ 7.80 (s, 1H, TzH), 7.75 (s, 1H, TzH*), 7.73 – 7.69 (m, 2H, Ar, Ar*), 7.45 (dd, *J* = 8.5, 2.3 Hz, 1H, Ar), 7.36 (dd, *J* = 8.5, 2.3 Hz, 1H, Ar*), 7.19 (d, *J* = 7.9 Hz, 2H, Ar), 7.17 – 7.08 (m, 3H, Ar, Ar*), 5.54 – 5.48 (m, 1H, CH), 5.45 (d, *J* =10 Hz, 1H, CH), 5.41 – 5.36 (m, 2H, CH_2), 5.34 (d, *J* = 9.7 Hz, 1H, CH_2), 5.25 (d, *J* = 4.8 Hz, 1H, CH), 4.97 (d, *J* = 11.0 Hz, 1H, CH_2), 4.86 (d, *J* = 11.2 Hz, 1H, CH_2), 4.70 (d, *J* = 11.2 Hz, 1H, CH_2), 4.62 (d, *J* = 4.7 Hz, 1H, CH), 4.56 (d, *J* = 1.6 Hz, 1H, CH), 4.10 (s, 3H, Me*), 3.89 (s, 3H, Me*), 3.77 – 3.71 (m, 2H, CH_2), 3.63 – 3.56 (m, 4H, CH_2, CH_2*), 3.41 – 3.34 (m, 1H, CH_2), 3.34 – 3.27 (m, 1H, CH_2), 1.32 – 1.28 (m, 12H, BPin, BPin*), 0.99 – 0.93 (m, 2H, CH_2), 0.90 – 0.83 (m, 2H, CH_2), 0.02 (s, 24H, $SiMe_3$*), -0.08 (s, 24H, $SiMe_3$); HRMS (ESI): m/z calcd for $C_{37}H_{54}BFN_6O_5Si_2Na$ $[M+Na]^+$, 771.36705; found, 771.36681.

*5-fluoro-9-(1-methyl-1H-1,2,4-triazol-5-yl)-8-(4-(tributylstannyl) phenyl)-2-((2-(trimethylsilyl)ethoxy)methyl)-2,7,8,9-tetrahydro-3H-pyrido[4,3,2-de]phthalazin-3-one (**7c**)*. The same general procedure was used to synthesize compound **7a** using compound **6a** (100 mg, 0.18 mmol), bis(tributyltin) (203 mg, 0.35 mmol), potassium acetate (98 mg, 0.525 mmol), and $Pd(dppf)Cl_2$ (13 mg, 0.02 mmol, 20 mol%) in DMF (3 ml). This afforded **7c** as an amorphous glass (60 mg, 44 %). ^{1}H NMR (600 MHz, $CDCl_3$): δ 7.81 (s, 1H), 7.45 – 7.38 (m, 3H), 7.28 – 7.23 (m, 2H), 6.70 (dd, *J* = 9.9, 2.4 Hz, 1H), 5.43 (d, *J* = 9.9 Hz, 1H), 5.25 (d, *J* = 9.9 Hz, 1H), 5.08 (d, *J* = 10.9 Hz, 1H), 4.93 (s, 1H), 4.49 (d, *J* = 10.9 Hz, 1H), 3.66 – 3.53 (m, 5H), 1.56 – 1.47 (m, 6H), 1.38 – 1.24 (m, 10H), 1.11 – 0.96 (m, 6H), 0.96 – 0.84 (m, 13H), -0.04 (s, 9H); ^{13}C NMR (151 MHz, $CDCl_3$): δ 165.82 (d, *J* = 252.1 Hz), 159.31, 152.10, 150.73, 146.98 (d, *J* = 12.2 Hz), 143.91, 140.14, 138.27, 137.15, 130.57, 126.79, 111.84, 104.26 (d, *J* = 27.5 Hz), 102.84 (d, *J* = 25.0 Hz), 79.64, 67.48, 60.78, 44.86, 35.18, 29.18, 27.44, 18.21, 13.80, 9.74, -1.25; HRMS (ESI): m/z calcd for $C_{37}H_{55}FN_6O_2SiSnNa$ $[M+Na]^+$, 805.30607; found, 805.30523.

Radiochemistry. All radiochemical reactions and experiments were carried out behind appropriate shielding per the rules and guidelines laid out in the German act on radiation protection (Strahlenschutzverordnung, StrlSchV). Radionuclides were produced using a PETtrace 890 (16 MeV protons) cyclotron (GE Healthcare, Uppsala, Sweden). ^{18}F was produced via the bombardment of [^{18}O]H_2O via the $^{18}O(p,n)^{18}F$ nuclear reaction and was delivered either as a target wash in H_2O (1.5-2.5 ml, 0.5-2 GBq/ml) for manual radiochemical experiments or in [^{18}O]H_2O (1.5-2.5 ml) through direct delivery from the cyclotron for automated synthesis (activity concentration dependent on bombardment time and beam current (10 min ≃ 34 GBq at 80 µA)). Automated ^{18}F tracer syntheses were performed on a either a GE FX N Pro synthesis module (GE Healthcare, Muenster, Germany) running the *TRACERlab* (GE) control and user-interface software or with an Elixys FLEX/CHEM radiosynthesizer coupled to an Elixys PURE/FORM purification and formulation module (Sofie Biosciences, Los Angeles, California, CA, USA) using proprietary Elixys FLEX/CHEM control software. Manual radiochemical experiments were performed using sealable single-use borosilicate glass reaction tubes (PYREX® 9 ml, corning, New York, NY, USA) with screw-top PTFE-lined caps. All reactions were stirred using either Teflon® or glass coated micro stirrer bars.

Radiochemical reaction performance was monitored using radioTLC on 0.20 mm Polygram SIL G/UV_{254} (silica gel 60) TLC plates. RadioTLC plates were developed with an appropriate running buffer/solvent mixture. RadioTLC data was acquired using a Cyclone Plus storage phosphor imaging system (PerkinElmer, Waltham, Massachusetts, USA). Analytical radio-HPLC data was collected using an Agilent HPLC (1260 Infinity series with an automated sample injector) coupled to an inline radiation detector (NaI(Tl)). In all cases, analytical radioHPLC data was obtained under the following general conditions unless otherwise stated: Column: Luna 5 µm C18 (2) 100 Å column (250 x 4.6 mm). The following gradient was run in all instances: Solvent A: H_2O + 0.1% TFA; Solvent B: MeCN; 0 - 2 min: (5% B); 0-17 min: (5 - 100% B); 17 - 23 min: (100% B); 23-28 min: (100-5% B).

For all radiochemical experiments, reagents, solvents, QMA eluents, reaction mixtures, and buffers were freshly prepared and dispensed directly before use unless otherwise stated.

^{18}F Processing. ^{18}F processing was carried out using a previously developed procedure:[39] Cyclotron-produced aqueous [^{18}F]fluoride was trapped on a QMA cartridge conditioned with aqueous KOTf (90 mg/ml). Residual water was blown off the cartridge using a stream of argon. ^{18}F was then eluted as [^{18}F]TBAF, using a solution of 10 mg TBAOTf in methanol (1 ml). The resulting methanolic [^{18}F]TBAF solution was transferred to a reactor vessel, either aliquoted for DoE optimization experiments or full batch tracer productions. This was followed by evaporation of the methanol under a stream of argon gas to afford dry [^{18}F]TBAF without the need for azeotropic drying.

General procedure. To dry [^{18}F]TBAF in a single-use glass reactor vessel was added a premade solution containing the required quantities of the precursor for radiolabeling (**7a-c**), $Cu(OTf)_2$, pyridine, DMA, and n-BuOH (total reaction volume of 700 µl). The reaction mixture was then stirred at 120 °C for 10 minutes before being quenched with HCl (0.25 M, 700 µl) or reacted further with 6 M HCl. Reaction performance was evaluated using radioTLC, which was read out using a Cyclone Plus storage phosphor imaging system (PerkinElmer, Waltham, Massachusetts, USA). Compound identity was confirmed by analytical radioHPLC against the non-radioactive standard compound.

DoE Studies and Validation. A computer-generated D-optimal DoE (design of experiments) study was designed and analyzed using *MODDE Go 12* (Sartorius, Göttingen, Germany). The D-optimal DoE study was performed to maximize the radiochemical yield of the CMRF step of the [^{18}F]talazoparib radiosynthesis across four experimental factors: The precursor load (*Pre*, 5-30 µmol), the copper-mediator load (*Cop*, 5-40 µmol), the pyridine load (*Py*, 20-500 µmol), and the % of *n*-BuOH co-solvent (*Bu*, 0-75%). The resulting worksheet table (Table S1) was used to calculate the required reactants, reagents, and solvents for each experiment, and the study was performed over 4 days using four cyclotron target washes. All DoE experiments were carried out in a randomized order. All reactions (tests and tracer productions) were carried out using a racemic mixture of protected (**7a**) precursor. In all cases, [^{18}F]fluoride was processed into [^{18}F]TBAF via the general procedure described above. The response (Y) was the %RCY of the labeling reaction and was measured by radioTLC (100% ethyl acetate development solvent). Selected runs were analyzed via radioHPLC against a non-radioactive standard (**6c**) to confirm compound identity.

Automated radiosynthesis. The detailed automated radiosynthesis of [^{18}F]talazoparib, using both the Elixys and FX N Pro systems, is described in detail in the Supplementary Information. The general procedure is as follows:

[^{18}F]Fluoride in [^{18}O]water was delivered into the module directly from the cyclotron, where it was trapped on a QMA cartridge (OTf-form). The [^{18}O]water was collected for recycling. The ^{18}F was then eluted with a solution of tetrabutylammonium triflate (TBAOTf) in methanol (1 ml), which was evaporated to dryness under a stream of argon to afford base-free [^{18}F]TBAF.[39] The DoE optimized reaction mixture, consisting of **7a** (19 mg, 30 µmol), $Cu(OTf)_2$ (3 mg, 5 µmol), and pyridine (24 µl, 300 µmol) in 700 µl DMA with *n*-BuOH (10%), was then added to the [^{18}F]TBAF and reacted at 120 °C for 20 min. After cooling the reactor vessel to ambient temperature, HCl (6 M, 700 µl) was added to the mixture and reacted at 120 °C for 15 min. The reaction vessel was again cooled, and the reaction was quenched with the addition of ammonium formate solution (25 mM, 5-10 ml dependent on the reactor vessel volume) containing NaOH (6 M, 600 µl). The mixture was then passed over an HLB SPE cartridge, trapping the product. The product was then eluted into a 5 ml vessel with acetonitrile (1 ml) and HLPC buffer (4 ml), and this solution was transferred to the first HPLC injection loop (5 ml). The product racemate was then isolated (retention time = 12-13 min) from the reaction mixture using reversed-phase HPLC (C18 Luna (10 µm, 10 × 250 mm)) via an isocratic method using water (0.1% TFA): acetonitrile (72:28) at a flow rate of 6 ml/min at room temperature. The radioactive fraction was collected in a sealed v-vial that was subsequently pressurized to load the solution onto a second HPLC injection loop. The purified racemic product was then injected onto a semipreparative CHIRALPAK IB-N5 (5 µm, 10 × 250 mm) HPLC column for enantiomeric resolution (water (0.1% TFA): acetonitrile (60:40); 5 ml/min, room temperature). The radioactive fraction corresponding to [^{18}F]talazoparib (retention time ≈ 12-13 min) or [^{18}F]LT-674 (retention time ≈ 14-15 min) was collected in a dilution reservoir, the contents of which were subsequently passed over an HLB cartridge. The product [^{18}F]talazoparib (or [^{18}F]LT-674) was eluted from the cartridge with ethanol (0.5 ml) and reconstituted with PBS (4.5 ml).

Quality control. Product identity was confirmed with analytical CHIRALPAK IB-N5 (5 µm, 4.6 × 150 mm) HPLC (water (0.1% TFA): acetonitrile (60:40); 1 ml/min, room temperature) against commercially acquired non-radioactive standard samples of talazoparib and its biologically inactive enantiomer LT-674. The molar activity of the radiotracer was calculated from the analytical HPLC UV signal using a calibration curve generated from the serial dilution of a standard sample of talazoparib.

In Vitro Uptake Studies. *Cell culture.* Human breast carcinoma cells (HCC1937, ACC513) were purchased from the German Collection of Microorganisms and Cell Cultures (DSMZ GmbH, Braunschweig, Germany) and cultured in Roswell Park Memorial Institute (RPMI) 1640 medium supplemented with 16 % fetal calf serum (FCS), 100 U/ml penicillin and 100 µg/ml streptomycin at 37°C under humid 5 % CO_2 atmosphere. The absence of mycoplasma infection was confirmed by PCR analysis in monthly intervals.

In vitro radiotracer uptake. HCC1937 cells (0.2×10^6) were incubated in 96-well filter plates (MADVN6550, Merck Millipore, Darmstadt, Germany) with 60 µl of a 0.4 MBq/ml radiotracer solution containing either 2.5 µl DMSO as vehicle, 2.5 µl 10 mM olaparib or 2.5 µl talazoparib to a final concentration of 25 µM for blocking. After 30 min of incubation at 37 °C, the cells were washed by vacuum filtration of the medium through the plate (2×100 µl followed by 2×200 µl), the filters were transferred into tubes using a commercial punch kit (MAMP09608, Merck) and measured in a gamma counter (Wizard 2, PerkinElmer, Waltham, MA, USA). Experiments were performed in triplicates, and the uptake was quantified as percent of added activity.

Competition assays. HCC1937 cells (0.2×10^6) were incubated in 96-well filter plates (MADVN6550, Merck Millipore, Darmstadt, Germany) with 40 µl of a 0.4 MBq/ml radiotracer and 20 µl of a 1:2 serial dilution of either talazoparib or olaparib starting with a final concentration of 1 µM. After 30 min of incubation at 37 °C, the cells were washed by vacuum filtration of the medium through the plate (2×100 µl followed by 2×200 µl), the filters were transferred into tubes using a commercial punch kit (MAMP09608, Merck) and measured in a gamma counter (Wizard 2, PerkinElmer). Experiments were performed in triplicates, and the uptake was quantified as percent of added activity.

In Vivo Evaluation. *PET and MR imaging.* All animal experiments were performed according to the German animal welfare act and approved by the local authorities (Regierungspraesidium Tuebingen, R3/18). Animals were housed in individually ventilated cages (IVCs, 5 mice per cage) with bedding and enrichment, and food and water provided *ad libitum*. Animals

were kept under isoflurane anesthesia (1.5 % in medical oxygen, 1.5 l/min) during all experiments. 1×10^7 cells in 1:1 ice-cold Matrigel (Thermo Scientific) / PBS were injected subcutaneously in the right shoulder area of 7 weeks-old female NOD.CB17-Prkdc^{scid}/J mice (n = 5). After the xenografts reached a suitable size (215.1 ± 72.8 mm^3), mice were injected with 13.12 ± 0.71 MBq [^{18}F]talazoparib and subjected to 1-hour dynamic PET imaging (Inveon D-PET, Siemens, Knoxville, TN, USA) with subsequent MR anatomical scans using a 7 Tesla Biospec 70/30 USR (Clinscan, Bruker Biospin) and a T2-weighted spin-echo sequence. The mice underwent a second, 10 min static PET scan 2 hours post-injection (p.i.). Mice were sacrificed by cervical dislocation. The collected organs were weighed, the tissue uptake was determined by gamma-counting (WIZARD2, PerkinElmer) and quantified as % of injected dose per gram (%ID/g). PET image reconstruction and correlation with the corresponding MR image were performed with Inveon Acquisition Workplace and Inveon Research Workplace, respectively, using a user-defined dynamic framing and an ordered subset expectation maximization (OSEM3D) algorithm. Regions of interest (ROIs) were drawn according to the acquired MR images and co-registered with the PET data to obtain time-activity curves (TACs).

Ex Vivo. *Immunofluorescence.* Immunofluorescence staining was performed by the Department of Dermatology at the University Hospital Tuebingen, Germany. Sections of paraffin-embedded xenografts were blocked with donkey serum for 30 min and incubated with primary antibody overnight (rabbit anti-PARP (1:50, ab74290, Abcam, Cambridge, UK)). After washing, the sections were incubated for 1 hour at room temperature with a secondary antibody (donkey anti-mouse IgG Cy3 (1:250, 715-166-151 Dianova, Hamburg, Germany). Nuclei were stained with YO-PRO-1 iodide solution (Y3603, Thermo Scientific) for 5 min; the samples were subsequently mounted with Mowiol (Sigma-Aldrich) and imaged on an LSM 800 microscope (Carl Zeiss, Oberkochen, Germany).

Statistical analyses. Statistical analyses were performed with GraphPad Prism 9 (GraphPad, La Jolla, CA, USA) using nonparametric t-tests and are represented as mean value ± standard deviation. Blood half-life was calculated using a two-phase decay fit. P-values < 0.05 were considered statistically significant according to the software (*: $p < 0.05$, **: $p < 0.01$, ***: $p < 0.001$, ****: $p < 0.0001$).

AUTHOR INFORMATION

Corresponding Author

Andreas Maurer[†,#,*]

Present Addresses

[†]Werner Siemens Imaging Center, Department of Preclinical Imaging and Radiopharmacy, Eberhard Karls University, Roentgenweg 15, 72076 Tuebingen, Germany

[#]Cluster of Excellence iFIT (EXC 2180) "Image-Guided and Functionally Instructed Tumor Therapies", Eberhard Karls University, Roentgenweg 13, 72076 Tuebingen, Germany

[§]Institute of Pharmaceutical Sciences, Department of Pharmaceutical (Bio-)Analysis, Eberhard Karls University, Auf der Morgenstelle 8, 72076 Tuebingen, Germany

^German Cancer Research Center, German Cancer Consortium DKTK, Partner Site Tuebingen, Roentgenweg 13, 72076 Tuebingen, Germany

Author Contributions

The study was designed by AM, BJP, GDB, and SS. Organic synthesis, radiosynthesis, and the analysis of the (radio)chemical DoE data was performed by GDB. ML and CG established the protocol for the chiral separation. *In vitro* and *in vivo* experiments and data analysis were performed by SS. SS, GDB, and AM wrote the first draft of the manuscript. All authors commented on previous versions of the manuscript. All authors read and approved the final version of the manuscript.

‡These authors contributed equally.

Funding Sources

This work was supported by the Werner Siemens Foundation (WSS) and parts of this work were funded by the Deutsche Forschungsgemeinschaft (DFG, German Research Foundation) under Germany's Excellence Strategy - EXC 2180 – 390900677.

Subject to priority patent applications (European patent application 21 173 663.2 and 21 173 674.9).

ACKNOWLEDGMENT

The authors want to thank Birgit Fehrenbacher and her team from the Department of Dermatology for IF staining, Ramona Stremme for assistance with the radiosyntheses as well as Siaolan Huang and Karl Mau for assistance with the animal studies. We would also like to thank Dr. Dorothee Wistuba and her colleagues at the mass spectroscopy core facility at the University of Tübingen, Germany. We would also like to thank Dr. Gerald Reischl and colleagues in the radiopharmacy at the Werner Siemens Imaging Center for the delivery of [^{18}F]fluoride and for technical support.

REFERENCES

1. Bryant, H. E.; Schultz, N.; Thomas, H. D.; Parker, K. M.; Flower, D.; Lopez, E.; Kyle, S.; Meuth, M.; Curtin, N. J.; Helleday, T., Specific killing of BRCA2-deficient tumours with inhibitors of poly(ADP-ribose) polymerase. *Nature* **2005,** *434* (7035), 913-7.
2. Farmer, H.; McCabe, N.; Lord, C. J.; Tutt, A. N.; Johnson, D. A.; Richardson, T. B.; Santarosa, M.; Dillon, K. J.; Hickson, I.; Knights, C.; Martin, N. M.; Jackson, S. P.; Smith, G. C.; Ashworth, A., Targeting the DNA repair defect in BRCA mutant cells as a therapeutic strategy. *Nature* **2005,** *434* (7035), 917-21.
3. Schoder, H.; Franca, P. D. S.; Nakajima, R.; Burnazi, E.; Roberts, S.; Brand, C.; Grkovski, M.; Mauguen, A.; Dunphy, M. P.; Ghossein, R. A.; Lyashchenko, S. K.; Lewis, J. S.; O'Donoghue, J. A.; Ganly, I.; Patel, S. G.; Lee, N. Y.; Reiner, T., Safety and Feasibility of PARP1/2 Imaging with (18)F-PARPi in Patients with Head and Neck Cancer. *Clin Cancer Res* **2020,** *26* (13), 3110-3116.
4. Siraj, A. K.; Pratheeshkumar, P.; Parvathareddy, S. K.; Divya, S. P.; Al-Dayel, F.; Tulbah, A.; Ajarim, D.; Al-Kuraya, K. S., Overexpression of PARP is an independent prognostic marker for poor survival in Middle Eastern breast cancer and its inhibition can be enhanced with embelin co-treatment. *Oncotarget* **2018,** *9* (99), 37319-37332.
5. Li, X.; Li, C.; Jin, J.; Wang, J.; Huang, J.; Ma, Z.; Huang, X.; He, X.; Zhou, Y.; Xu, Y.; Yu, M.; Huang, S.; Yan, X.; Li, F.; Pan, J.; Wang, Y.; Yu, Y.; Jin, J., High PARP-1 expression predicts poor survival in acute myeloid leukemia and PARP-1 inhibitor and SAHA-bendamustine hybrid inhibitor combination treatment synergistically enhances anti-tumor effects. *EBioMedicine* **2018,** *38*, 47-56.
6. Bertucci, F.; Finetti, P.; Monneur, A.; Perrot, D.; Chevreau, C.; Le Cesne, A.; Blay, J. Y.; Mir, O.; Birnbaum, D., PARP1 expression in soft tissue sarcomas is a poor-prognosis factor and a new potential therapeutic target. *Mol Oncol* **2019,** *13* (7), 1577-1588.
7. Gradwohl, G.; Menissier de Murcia, J. M.; Molinete, M.; Simonin, F.; Koken, M.; Hoeijmakers, J. H.; de Murcia, G., The second zinc-finger domain of poly(ADP-ribose) polymerase determines specificity for single-stranded breaks in DNA. *Proc Natl Acad Sci U S A* **1990,** *87* (8), 2990-4.
8. Langelier, M. F.; Planck, J. L.; Roy, S.; Pascal, J. M., Structural basis for DNA damage-dependent poly(ADP-ribosyl)ation by human PARP-1. *Science* **2012,** *336* (6082), 728-32.
9. Rouleau, M.; Patel, A.; Hendzel, M. J.; Kaufmann, S. H.; Poirier, G. G., PARP inhibition: PARP1 and beyond. *Nat Rev Cancer* **2010,** *10* (4), 293-301.
10. Langelier, M. F.; Eisemann, T.; Riccio, A. A.; Pascal, J. M., PARP family enzymes: regulation and catalysis of the poly(ADP-ribose) posttranslational modification. *Curr Opin Struct Biol* **2018,** *53*, 187-198.
11. Vyas, S.; Matic, I.; Uchima, L.; Rood, J.; Zaja, R.; Hay, R. T.; Ahel, I.; Chang, P., Family-wide analysis of poly(ADP-ribose) polymerase activity. *Nat Commun* **2014,** *5*, 4426.
12. Eisemann, T.; Pascal, J. M., Poly(ADP-ribose) polymerase enzymes and the maintenance of genome integrity. *Cell Mol Life Sci* **2020,** *77* (1), 19-33.
13. Langelier, M. F.; Zandarashvili, L.; Aguiar, P. M.; Black, B. E.; Pascal, J. M., NAD(+) analog reveals PARP-1 substrate-blocking mechanism and allosteric communication from catalytic center to DNA-binding domains. *Nat Commun* **2018,** *9* (1), 844.
14. Javle, M.; Curtin, N. J., The role of PARP in DNA repair and its therapeutic exploitation. *Br J Cancer* **2011,** *105* (8), 1114-22.
15. Francica, P.; Rottenberg, S., Mechanisms of PARP inhibitor resistance in cancer and insights into the DNA damage response. *Genome Med* **2018,** *10* (1), 101.
16. Kim, G.; Ison, G.; McKee, A. E.; Zhang, H.; Tang, S.; Gwise, T.; Sridhara, R.; Lee, E.; Tzou, A.; Philip, R.; Chiu, H. J.; Ricks, T. K.; Palmby, T.; Russell, A. M.; Ladouceur, G.; Pfuma, E.; Li, H.; Zhao, L.; Liu, Q.; Venugopal, R.; Ibrahim, A.; Pazdur, R., FDA Approval Summary: Olaparib Monotherapy in Patients with Deleterious Germline BRCA-Mutated Advanced Ovarian Cancer Treated with Three or More Lines of Chemotherapy. *Clin Cancer Res* **2015,** *21* (19), 4257-61.
17. Dockery, L. E.; Gunderson, C. C.; Moore, K. N., Rucaparib: the past, present, and future of a newly approved PARP inhibitor for ovarian cancer. *Onco Targets Ther* **2017,** *10*, 3029-3037.
18. Scott, L. J., Niraparib: First Global Approval. *Drugs* **2017,** *77* (9), 1029-1034.
19. Hoy, S. M., Talazoparib: First Global Approval. *Drugs* **2018,** *78* (18), 1939-1946.

20. Keung, M. Y.; Wu, Y.; Badar, F.; Vadgama, J. V., Response of Breast Cancer Cells to PARP Inhibitors Is Independent of BRCA Status. *J Clin Med* **2020,** *9* (4).

21. Lord, C. J.; Ashworth, A., PARP inhibitors: Synthetic lethality in the clinic. *Science* **2017,** *355* (6330), 1152-1158.

22. Carney, B.; Kossatz, S.; Lok, B. H.; Schneeberger, V.; Gangangari, K. K.; Pillarsetty, N. V. K.; Weber, W. A.; Rudin, C. M.; Poirier, J. T.; Reiner, T., Target engagement imaging of PARP inhibitors in small-cell lung cancer. *Nat Commun* **2018,** *9* (1), 176.

23. Shen, Y.; Rehman, F. L.; Feng, Y.; Boshuizen, J.; Bajrami, I.; Elliott, R.; Wang, B.; Lord, C. J.; Post, L. E.; Ashworth, A., BMN 673, a novel and highly potent PARP1/2 inhibitor for the treatment of human cancers with DNA repair deficiency. *Clin Cancer Res* **2013,** *19* (18), 5003-15.

24. Wang, B.; Chu, D.; Feng, Y.; Shen, Y.; Aoyagi-Scharber, M.; Post, L. E., Discovery and Characterization of (8S,9R)-5-Fluoro-8-(4-fluorophenyl)-9-(1-methyl-1H-1,2,4-triazol-5-yl)-2,7,8,9-te trahydro-3H-pyrido[4,3,2-de]phthalazin-3-one (BMN 673, Talazoparib), a Novel, Highly Potent, and Orally Efficacious Poly(ADP-ribose) Polymerase-1/2 Inhibitor, as an Anticancer Agent. *J Med Chem* **2016,** *59* (1), 335-57.

25. Pommier, Y.; O'Connor, M. J.; de Bono, J., Laying a trap to kill cancer cells: PARP inhibitors and their mechanisms of action. *Sci Transl Med* **2016,** *8* (362), 362ps17.

26. Carlucci, G.; Carney, B.; Brand, C.; Kossatz, S.; Irwin, C. P.; Carlin, S. D.; Keliher, E. J.; Weber, W.; Reiner, T., Dual-Modality Optical/PET Imaging of PARP1 in Glioblastoma. *Mol Imaging Biol* **2015,** *17* (6), 848-55.

27. Kossatz, S.; Brand, C.; Gutiontov, S.; Liu, J. T.; Lee, N. Y.; Gonen, M.; Weber, W. A.; Reiner, T., Detection and delineation of oral cancer with a PARP1 targeted optical imaging agent. *Sci Rep* **2016,** *6*, 21371.

28. Kossatz, S.; Pirovano, G.; Demetrio De Souza Franca, P.; Strome, A. L.; Sunny, S. P.; Zanoni, D. K.; Mauguen, A.; Carney, B.; Brand, C.; Shah, V.; Ramanajinappa, R. D.; Hedne, N.; Birur, P.; Sihag, S.; Ghossein, R. A.; Gonen, M.; Strome, M.; Suresh, A.; Molena, D.; Ganly, I.; Kuriakose, M. A.; Patel, S. G.; Reiner, T., Validation of the use of a fluorescent PARP1 inhibitor for the detection of oral, oropharyngeal and oesophageal epithelial cancers. *Nat Biomed Eng* **2020,** *4* (3), 272-285.

29. Michel, L. S.; Dyroff, S.; Brooks, F. J.; Spayd, K. J.; Lim, S.; Engle, J. T.; Phillips, S.; Tan, B.; Wang-Gillam, A.; Bognar, C.; Chu, W.; Zhou, D.; Mach, R. H.; Laforest, R.; Chen, D. L., PET of Poly (ADP-Ribose) Polymerase Activity in Cancer: Preclinical Assessment and First In-Human Studies. *Radiology* **2017,** *282* (2), 453-463.

30. Edmonds, C. E.; Makvandi, M.; Lieberman, B. P.; Xu, K.; Zeng, C.; Li, S.; Hou, C.; Lee, H.; Greenberg, R. A.; Mankoff, D. A.; Mach, R. H., [(18)F]FluorThanatrace uptake as a marker of PARP1 expression and activity in breast cancer. *Am J Nucl Med Mol Imaging* **2016,** *6* (1), 94-101.

31. Young, R. J.; Demetrio De Souza Franca, P.; Pirovano, G.; Piotrowski, A. F.; Nicklin, P. J.; Riedl, C. C.; Schwartz, J.; Bale, T. A.; Donabedian, P. L.; Kossatz, S.; Burnazi, E. M.; Roberts, S.; Lyashchenko, S. K.; Miller, A. M.; Moss, N. S.; Fiasconaro, M.; Zhang, Z.; Mauguen, A.; Reiner, T.; Dunphy, M. P., Preclinical and first-in-human-brain-cancer applications of [(18)F]poly (ADP-ribose) polymerase inhibitor PET/MR. *Neurooncol Adv* **2020,** *2* (1), vdaa119.

32. Kossatz, S.; Carney, B.; Farley, C.; Weber, W. A.; Drain, C. M.; Reiner, T., Direct Imaging of Drug Distribution and Target Engagement of the PARP Inhibitor Rucaparib. *J Nucl Med* **2018,** *59* (8), 1316-1320.

33. Carney, B.; Kossatz, S.; Reiner, T., Molecular Imaging of PARP. *J Nucl Med* **2017,** *58* (7), 1025-1030.

34. Wright, J. S.; Kaur, T.; Preshlock, S.; Tanzey, S. S.; Winton, W. P.; Sharninghausen, L. S.; Wiesner, N.; Brooks, A. F.; Sanford, M. S.; Scott, P. J. H., Copper-Mediated Late-stage Radiofluorination: Five Years of Impact on Pre-clinical and Clinical PET Imaging. *Clin Transl Imaging* **2020,** *8* (3), 167-206.

35. Tredwell, M.; Preshlock, S. M.; Taylor, N. J.; Gruber, S.; Huiban, M.; Passchier, J.; Mercier, J.; Genicot, C.; Gouverneur, V., A general copper-mediated nucleophilic 18F fluorination of arenes. *Angew Chem Int Ed Engl* **2014,** *53* (30), 7751-5.

36. Makaravage, K. J.; Brooks, A. F.; Mossine, A. V.; Sanford, M. S.; Scott, P. J. H., Copper-Mediated Radiofluorination of Arylstannanes with [(18)F]KF. *Org Lett* **2016,** *18* (20), 5440-5443.

37. Mossine, A. V.; Brooks, A. F.; Makaravage, K. J.; Miller, J. M.; Ichiishi, N.; Sanford, M. S.; Scott, P. J., Synthesis of [18F]Arenes via the Copper-Mediated [18F]Fluorination of Boronic Acids. *Org Lett* **2015,** *17* (23), 5780-3.

38. Bowden, G. D.; Pichler, B. J.; Maurer, A., A Design of Experiments (DoE) Approach Accelerates the Optimization of Copper-Mediated (18)F-Fluorination Reactions of Arylstannanes. *Sci Rep* **2019,** *9* (1), 11370.

39. Bowden, G. D.; Chailanggar, N.; Pichler, B. J.; Maurer, A., Scalable ^{18}F Processing Conditions for Copper-Mediated Radiofluorination Chemistry Facilitate "Design of Experiments" (DoE) Optimization Studies and Afford an Improved Synthesis of [^{18}F]Olaparib. *Preprint, doi: 10.26434/chemrxiv.14547342.v1*. 2021.

40. Taylor, N. J.; Emer, E.; Preshlock, S.; Schedler, M.; Tredwell, M.; Verhoog, S.; Mercier, J.; Genicot, C.; Gouverneur, V., Derisking the Cu-Mediated (18)F-Fluorination of Heterocyclic Positron Emission Tomography Radioligands. *J Am Chem Soc* **2017,** *139* (24), 8267-8276.

41. Zlatopolskiy, B. D.; Zischler, J.; Krapf, P.; Zarrad, F.; Urusova, E. A.; Kordys, E.; Endepols, H.; Neumaier, B., Copper-mediated aromatic radiofluorination revisited: efficient production of PET tracers on a preparative scale. *Chemistry* **2015,** *21* (15), 5972-9.

42. Albrecht, B. K.; Bauer, D.; Bellon, S.; Bode, C. M.; Booker, S.; Boezio, A.; Choquette, D.; D'Amico, D.; Harmange, J.-C.; Hirai, S.; Hungate, R. W.; Kim, T.-S.; Lewis, R. T.; Liu, L.; Lohman, J.; Norman, M. H.; Potashman, M.; Siegmund, A. C.; Springer, S. K.; Stec, M.; Xi, N.; Yang, K. Fused Heterocyclic Derivatives and Methods of Use, WO2009091374. 2009.

43. Wilson, T. C.; Xavier, M. A.; Knight, J.; Verhoog, S.; Torres, J. B.; Mosley, M.; Hopkins, S. L.; Wallington, S.; Allen, P. D.; Kersemans, V.; Hueting, R.; Smart, S.; Gouverneur, V.; Cornelissen, B., PET Imaging of PARP Expression Using (18)F-Olaparib. *J Nucl Med* **2019,** *60* (4), 504-510.

44. Guibbal, F.; Isenegger, P. G.; Wilson, T. C.; Pacelli, A.; Mahaut, D.; Sap, J. B. I.; Taylor, N. J.; Verhoog, S.; Preshlock, S.; Hueting, R.; Cornelissen, B.; Gouverneur, V., Manual and automated Cu-mediated radiosynthesis of the PARP inhibitor [(18)F]olaparib. *Nat Protoc* **2020,** *15* (4), 1525-1541.

45. Zischler, J.; Kolks, N.; Modemann, D.; Neumaier, B.; Zlatopolskiy, B. D., Alcohol-Enhanced Cu-Mediated Radiofluorination. *Chemistry* **2017,** *23* (14), 3251-3256.

46. Ryan, K.; Bolanos, B.; Smith, M.; Palde, P.; Cuenca, P. D.; VanArsdale, T. L.; Niessen, S.; Zhang, L.; Behenna, D.; Ornelas, M. A.; Tran, K. T.; Kaiser, S.; Lum, L.; Stewart, A.; Gajiwala, K. S., Dissecting the molecular determinants of clinical PARP1 inhibitor selectivity for tankyrase1. *J Biol Chem* **2021**, 100251.

47. Carney, B.; Carlucci, G.; Salinas, B.; Di Gialleonardo, V.; Kossatz, S.; Vansteene, A.; Longo, V. A.; Bolaender, A.; Chiosis, G.; Keshari, K. R.; Weber, W. A.; Reiner, T., Non-invasive PET Imaging of PARP1 Expression in Glioblastoma Models. *Mol Imaging Biol* **2016,** *18* (3), 386-92.